Hindawi
Advances in Civil Engineering
Volume 2018, Article ID 5406931, 12 pages
https://doi.org/10.1155/2018/5406931

Research Article

Stress Uniformity Analyses on Nonparallel End-Surface Rock Specimen during Loading Process in SHPB Tests

Pu Yuan,[1,2] **Qin-yong Ma**,[1,2,3] **and Dong-dong Ma**[1]

[1]*School of Civil Engineering and Architecture, Anhui University of Science and Technology, Huainan 232001, China*
[2]*Engineering Research Center of Underground Mine Construction, Ministry of Education, Anhui University of Science and Technology, Huainan 232001, China*
[3]*State Key Laboratory of Mining Disaster Prevention and Control Co-Founded by Shandong Province and the Ministry of Science and Technology, Shandong University of Science and Technology, Qingdao 266590, China*

Correspondence should be addressed to Pu Yuan; puy2012@126.com

Received 31 January 2018; Revised 27 April 2018; Accepted 30 May 2018; Published 11 July 2018

Academic Editor: Wei Wu

To investigate the influence of nonparallel end-surface on stress uniformity during loading process in rock SHPB test, SHPB numerical simulations have been carried out by LS-DYNA when end-face nonparallelism is within 0.40% and Young's modulus ranges from 14 GPa to 42 GPa. Isotropic linear elastic model is applied for elastic steel pressure bar, and HJC constitutive model is chosen for rock specimen. Numerical simulation results indicate that fluctuation effect exists in both reflected stress waves and transmitted stress waves, and it is enhanced with the increase of end-surface nonparallelism. The stress nonuniformity coefficient attenuates in a serrated fluctuation. With the increase of end-surface nonparallelism, the amplitude of transmitted stress wave gradually reduces, while stress nonuniformity coefficient increases. Stress equilibrium time first decreases slightly then increases in a step type. Therefore, nonparallel end-surface leads to two reverse results for stress uniformity during SHPB loading process, extending stress equilibrium time and shortening stress equilibrium time. And the influence on shortening stress equilibrium time is weak, while the influence on extending stress equilibrium time is great. When end-surface nonparallelism is 0.10%, stress equilibrium time achieves its lowest value whatever Young's modulus is. Hence, end-surface nonparallelism of the rock specimen is suggested to be controlled within 0.10% when conducting SHPB tests.

1. Introduction

Split Hopkinson pressure bar (SHPB) apparatus has been a very popular and promising experimental technique for evaluating the dynamic mechanical characteristics of rock [1, 2], concrete [3], soil [4], and cemented sand [5] at high strain rates (10^2~10^4 s^{-1}). Conventional SHPB apparatus consists of three essential parts: a striker bar, an incident bar, and a transmission bar. A pending specimen is sandwiched between the incident bar and transmission bar. Therefore, there are three contact surfaces in SHPB tests: the contact surface between the striker and incident bars, the contact surface between the incident bar and the pending specimen, and the contact surface between the transmission bar and the pending specimen [6]. Parallel condition and friction situation of three contact surfaces play a great impact on dynamic mechanical characteristics of pending specimen in SHPB tests [7–9].

With the development of SHPB technique, how to improve the accuracy of SHPB test results and the precision of dynamic mechanical characteristics measurement is becoming a key issue for SHPB technique [6]. For SHPB apparatus, there are two kinds of bar misalignment effect: processing accuracy and assembly precision of elastic pressure bars. Six major types of bar misalignment, offset of neutral axis, uneven support height, nonparallel impact end-surface, bar straightness, dome, and cone impact end-surface shapes, have been investigated by numerical simulations, and the distorted signal generated by bar misalignment produces unreliable data analysis for the presence of a flexural mode of vibration [8]. To estimate the effects of imperfect conditions on incident waves in SHPB tests, four

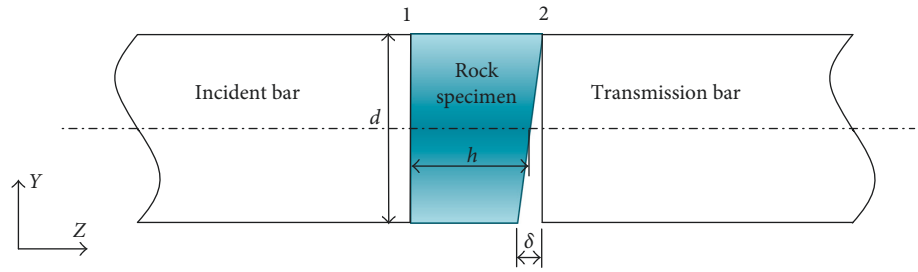

Figure 1: Nonparallel end-surface rock specimen.

types of imperfect conditions, curved bar, axis offset between the striker and incident bars, inclination of impact end-surface, and indentation of impact end-surface, have been investigated by numerical simulation, and inclination and indentation of impact end-surface present a great impact on incident wave [9]. For SHPB apparatus with special shape striker, axis offset and inclination of special shape striker lead to wave distortion and amplitude decrease, and system calibration of SHPB apparatus is classified into four steps: system adjustment, wave distortion identification, measurement calibration, and transmission calibration [10].

For SHPB apparatus, striker bar, incident bar, and transmission bar are factory calibrated and assembled coaxially before SHPB tests. Therefore, the influence of processing accuracy and assembly precision of elastic pressure bars can be ignored. For rock materials, each pending rock specimen is prepared into a short cylinder with length to diameter ratio of 0.5 through drilling, cutting, and grinding process [11, 12]. The processing accuracy is varied for rock specimen. For short cylinder rock specimen, the flatness of both end-surfaces can be within 0.02 mm, while the perpendicularity of two end-surfaces to the axis is difficult to be controlled [13]. Therefore, the nonparallel effect of rock specimen end-surface in SHPB tests should be investigated.

For rock-like materials, the validity of SHPB tests is based on no brittle failure before achieving stress equilibrium. To evaluate the influence of nonparallel end-surface on stress uniformity during loading process in rock SHPB tests, numerical simulation on SHPB tests for rock materials have been carried out by LS-DYNA when end-face nonparallelism is within 0.40% and Young's modulus ranges from 14 GPa to 42 GPa. Then both stress nonuniformity coefficient and stress equilibrium time are analyzed under various end-surface nonparallelism conditions.

2. Numerical Model of Rock SHPB Tests with Nonparallel End-Surface

2.1. Nonparallel End-Surface. In rock SHPB tests, the common size of rock specimen is $\Phi 50 \times 25$ mm. To simplify the analysis, it can be assumed that only one end-surface is not perpendicular to the rock specimen axis and the nonparallel end-surface is in contact with the transmission bar, which can be seen from Figure 1.

End-surface nonparallelism, marked as γ, is defined as the ratio of maximum height deviation δ to average height h of rock specimen [6, 13]. And it can be derived as

$$\gamma = \frac{\delta}{h} \times 100\%. \quad (1)$$

To explore the influence of end-surface nonparallelism on stress uniformity during loading process in rock SHPB tests, 9 kinds of end-surface nonparallelisms are involved for rock specimens, which are 0%, 0.05%, 0.10%, 0.15%, 0.20%, 0.25%, 0.30%, 0.35%, and 0.40%, respectively. Therefore, maximum height deviation δ varies from 0 to 0.100 mm.

2.2. Half-Sine Loading Waveform. For rock-like materials, half-sine loading waveform with a slow rising is an ideal loading waveform. The half-sine loading waveform not only attenuates oscillation and dispersion effect, but also achieves an approximate constant strain rate deformation [10]. During SHPB numerical simulation, a half-sine loading waveform with amplitude of 260 MPa and duration of 240 μs is directly applied on the impact end-surface of the incident bar.

2.3. Three-Dimensional Numerical Model of SHPB Tests. Finite element model of SHPB test is based on $\Phi 50$ mm steel SHPB test apparatus. A three-dimensional numerical model including incident bar, transmission bar, and rock specimen is set up in ANSYS. Then, a keyword file is output from ANSYS and revised by applying HJC model for the rock specimen. Finally, LS-DYNA is adopted to run the revised keyword and output SHPB numerical simulation results. In three-dimensional numerical model, both incident bar and transmission bar are straight bars with size of $\Phi 50 \times 2000$ mm, and their axial directions are along the Z-axis. The average height of rock specimen with nonparallel end-surface is 25 mm. According to the actual situation of SHPB apparatus, the incident bar, transmission bar, and rock specimen are constrained from X direction and Y direction. A hexahedral solid element SOLID164, defined by 8 nodes, is used for three-dimensional modeling. And the number of solid elements for the incident bar, transmission bar, and nonparallel end-surface rock specimen is all 60000. Three-dimensional numerical model including the incident bar, transmission bar, and rock specimen with nonparallel end-surface is shown in Figure 2.

2.4. Material Parameters for Rock Specimens and Elastic Steel Pressure Bar. Isotropic linear elastic model is applied for

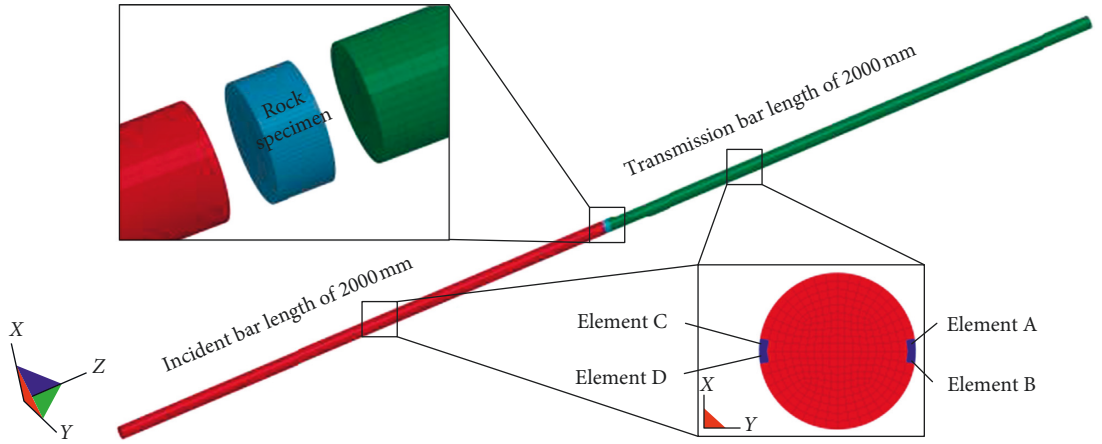

Figure 2: Three-dimensional numerical model including incident bar, transmission bar, and rock specimen.

Table 1: Material parameters for HJC model of rock material with Young's modulus of 14 GPa.

ρ (g/cm^3)	G (GPa)	f_c (MPa)	T (MPa)	A	B	C
2.47	5.83	130.00	7.07	0.79	1.60	0.007
N	S_{max}	D_1	D_2	ε_{fmin}	$\dot{\varepsilon}_0$ (s^{-1})	p_c (MPa)
0.61	4.0	0.045	1.0	0.005	1.0×10^{-6}	43.33
μ_c	p_{lock} (GPa)	μ_{lock}	K_1 (GPa)	K_2 (GPa)	K_3 (GPa)	f_s
0.00557	1	0.1	85	−171	208	0.004

elastic steel pressure bar. The density, Young's modulus, and Poisson's ratio for both the incident bar and transmission bar are 7.85 g/cm^3, 210 GPa, and 0.30 respectively.

Considering various Young's moduli of rock material, 5 kinds of Young's moduli are involved, which are 14 GPa, 21 GPa, 28 GPa, 35 GPa, and 42 GPa, respectively. Holmquist–Johnson–Cook (HJC) dynamic damage constitutive model is chosen for rock specimens [14]. In HJC model, only shear modulus G and crushing volumetric strain μ_c vary with Young's modulus and can be calculated by (2) and (3). The other parameters for HJC model of rock specimens keep constant for various Young's moduli. The density ρ and Poisson's ratio ν of rock material are 2.47 g/cm^3 and 0.20, respectively. f_c and T stand for quasistatic uniaxial compressive strength and maximum tensile hydrostatic pressure. A, B, C, N, and S_{max} are normalized cohesive strength, normalized pressure hardening coefficient, strain rate coefficient, pressure hardening exponent, and normalized maximum strength. $\dot{\varepsilon}_0$ and ε_{fmin} are reference strain rate and plastic strain before fracture. p_c, p_{lock}, μ_c, and μ_{lock} are crushing pressure, locking pressure, crushing volumetric strain, and locking volumetric strain. D_1 and D_2 are damage constants. K_1, K_2, and K_3 are material constants. f_s is failure type. When Young's modulus is 14 GPa, the material parameters for HJC model are listed in Table 1:

$$G = \frac{E}{2(1+\nu)}, \tag{2}$$

$$\mu_c = \frac{p_c}{K} = \frac{f_c(1-2\nu)}{E}. \tag{3}$$

3. SHPB Numerical Simulation Results of Nonparallel End-Surface Rock Specimens

3.1. Numerical Simulation Validation. SHPB technique is based on two fundamental assumptions. One is one-dimensional stress wave propagation, and the other is stress uniformity [1]. And the stress uniformity assumption is the key to validate a SHPB test and can be checked by comparing the stress histories on both ends of rock specimens or checking the unbalance stress during SHPB tests.

In SHPB tests, the incident stress $\sigma_I(t)$, reflected stress $\sigma_R(t)$, and transmitted stress $\sigma_T(t)$ are acquired by strain gauges mounted on the incident bar and transmission bar. Two strain gauges are mounted symmetrically on the surface of incident bar or transmission bar to eliminate the flexural vibration effect. As shown in Figure 2, four elements, A, B, C, and D, at the same cross section where two strain gauges mounted in actual SHPB tests are selected to export numerical simulation results for stress uniformity analyses. Two adjacent elements, A and B, correspond to maximum height point, and two adjacent elements, C and D, correspond to minimum height point. Four elements on the incident bar are 1000 mm away from the contact surface between the incident bar and rock specimen. While four elements on transmission bar are 400 mm away from the contact surface between the transmission bar and rock specimen. When Young's modulus is 28 GPa, the incident, reflected, transmitted, and unbalance stresses for the rock specimen with end-surface nonparallelism of 0% and 0.40% are shown in Figure 3. The unbalance stress can be calculated

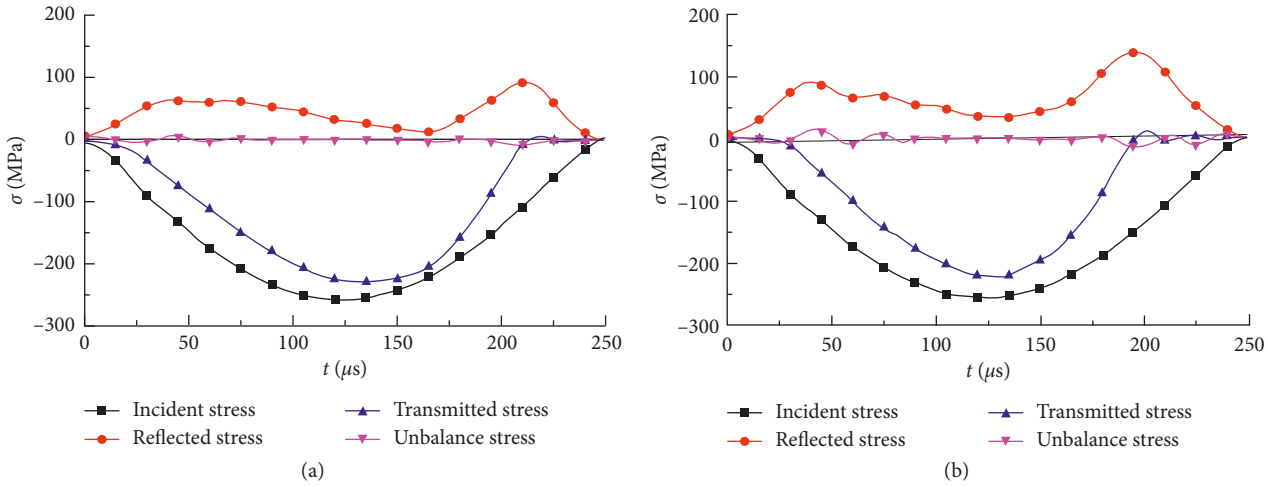

Figure 3: The incident, reflected, transmitted, and unbalance stresses when Young's modulus is 28 GPa: (a) $\gamma = 0\%$, and (b) $\gamma = 0.40\%$.

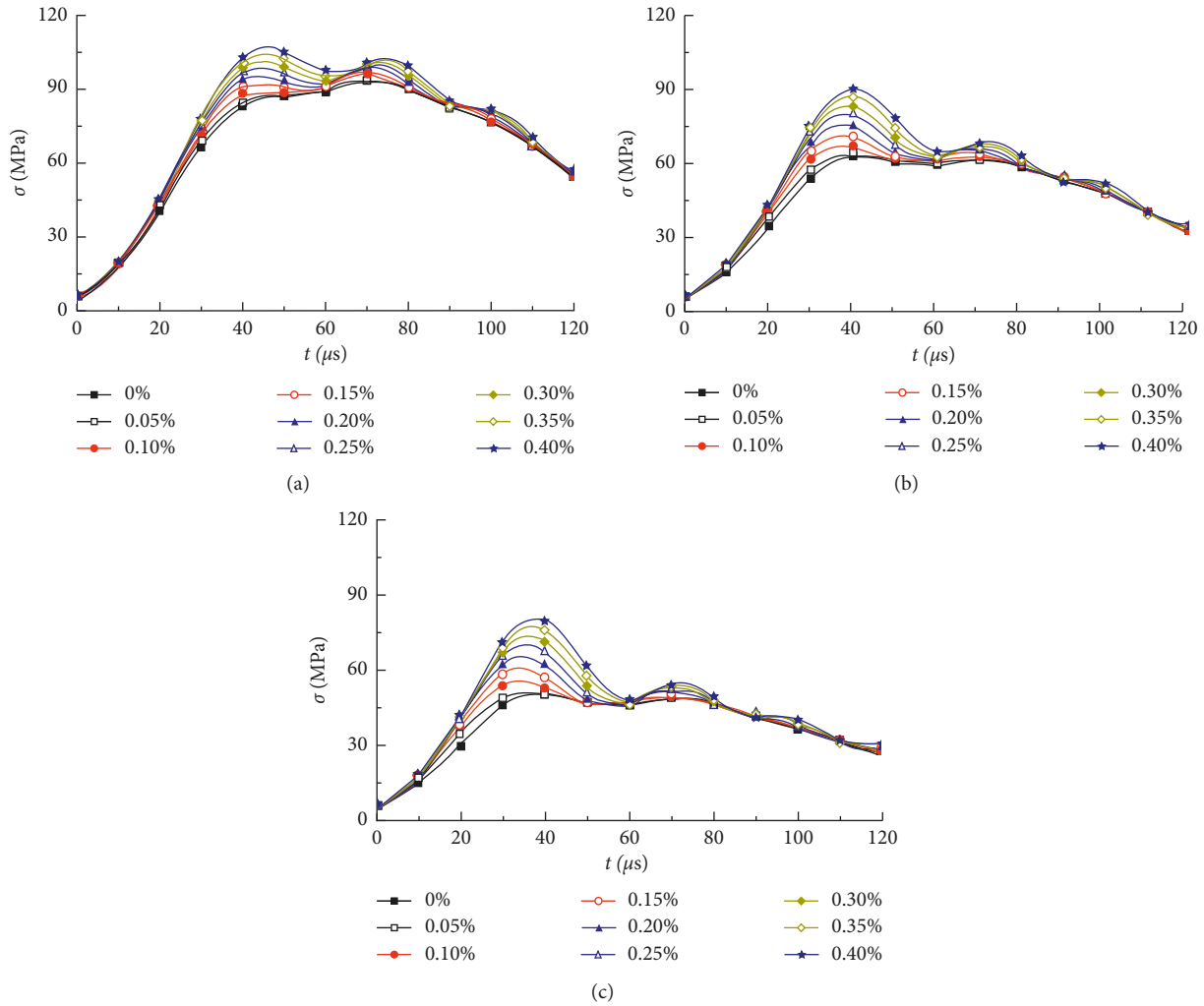

Figure 4: Reflected stresses of rock specimens for various end-surface nonparallelisms: (a) $E = 14$ GPa, (b) $E = 28$ GPa, and (c) $E = 42$ GPa.

by $\sigma_I(t) + \sigma_R(t) - \sigma_T(t)$. When rock specimen element failure occurs, the original contact between the incident bar and rock specimen does not exist and become a free end-surface. Hence, there are two peaks in reflected stress wave, one in loading process, and the other after the failure of rock specimen.

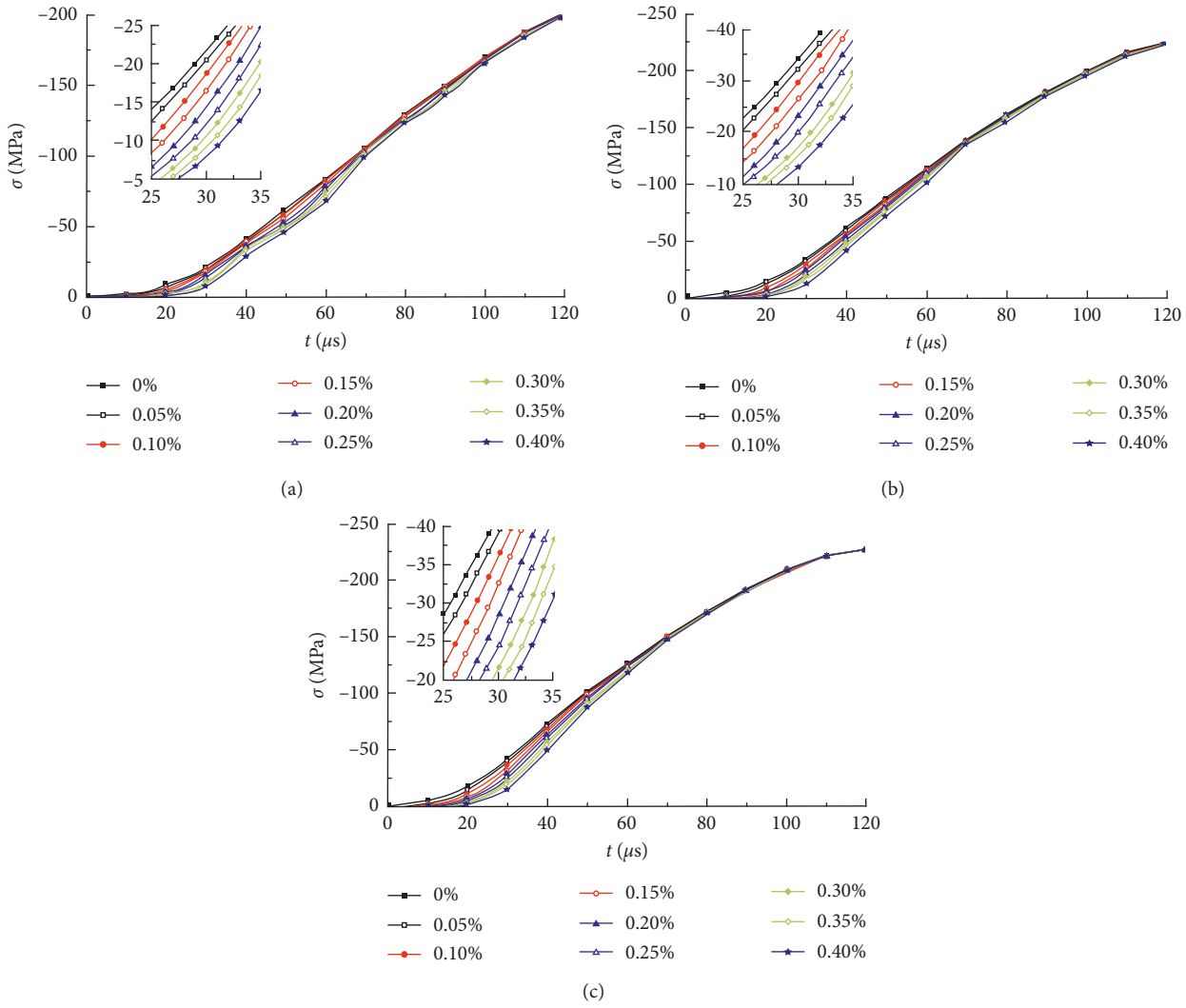

FIGURE 5: Transmitted stresses of rock specimens for various end-surface nonparallelisms: (a) $E = 14$ GPa, (b) $E = 28$ GPa, and (c) $E = 42$ GPa.

As shown in Figure 3, the unbalance stress for rock specimen with end-surface nonparallelism of 0% and 0.40% is very small and oscillates above and below 0. Relatively big fluctuation only appears at the initial part and end part of unbalance stress. Therefore, finite element model for rock SHPB tests is correct and can be used for the following analyses.

3.2. Reflected Stress Wave and Transmitted Stress Wave. According to one-dimensional stress wave theory, reflected wave and transmitted wave emerge when stress wave propagates to the contact surface between two materials with different wave impedances. And the area and geometry of contact surface show an impact on the reflected wave and transmitted wave [15]. Typical reflected stress and transmitted stress for various nonparallel end-surface rock specimens are shown in Figures 4 and 5. Considering the rising time of half-sine incident stress wave, the time of loading process in SHPB numerical simulation is 120 μs.

As shown in Figure 4, an obvious fluctuation presents in reflected stresses, especially in the middle part of the whole loading process. The fluctuation effect in reflected stresses is enhanced with end-surface nonparallelism and Young's modulus. The amplitude of reflected stresses for rock specimens gradually rises with the increase of end-surface nonparallelism and decreases with the increase of Young's modulus.

As shown in Figure 5, a slight fluctuation presents in transmitted stresses, especially in the middle part of the whole loading process. Both the amplitude and duration of fluctuation in transmitted stresses are enhanced with end-surface nonparallelism, whereas both the amplitude and duration of fluctuation in transmitted stresses are weakened with the increase of Young's modulus. The amplitude of transmitted stresses for various nonparallel end-surface rock specimens gradually decrease with the increase of end-surface nonparallelism and rise with the increase of Young's modulus.

Above all, fluctuation effect exists in both reflected stresses and transmitted stresses. For parallel end-surface rock specimens, reflected stress and transmitted stress propagate along the axis for an entire circular contact area.

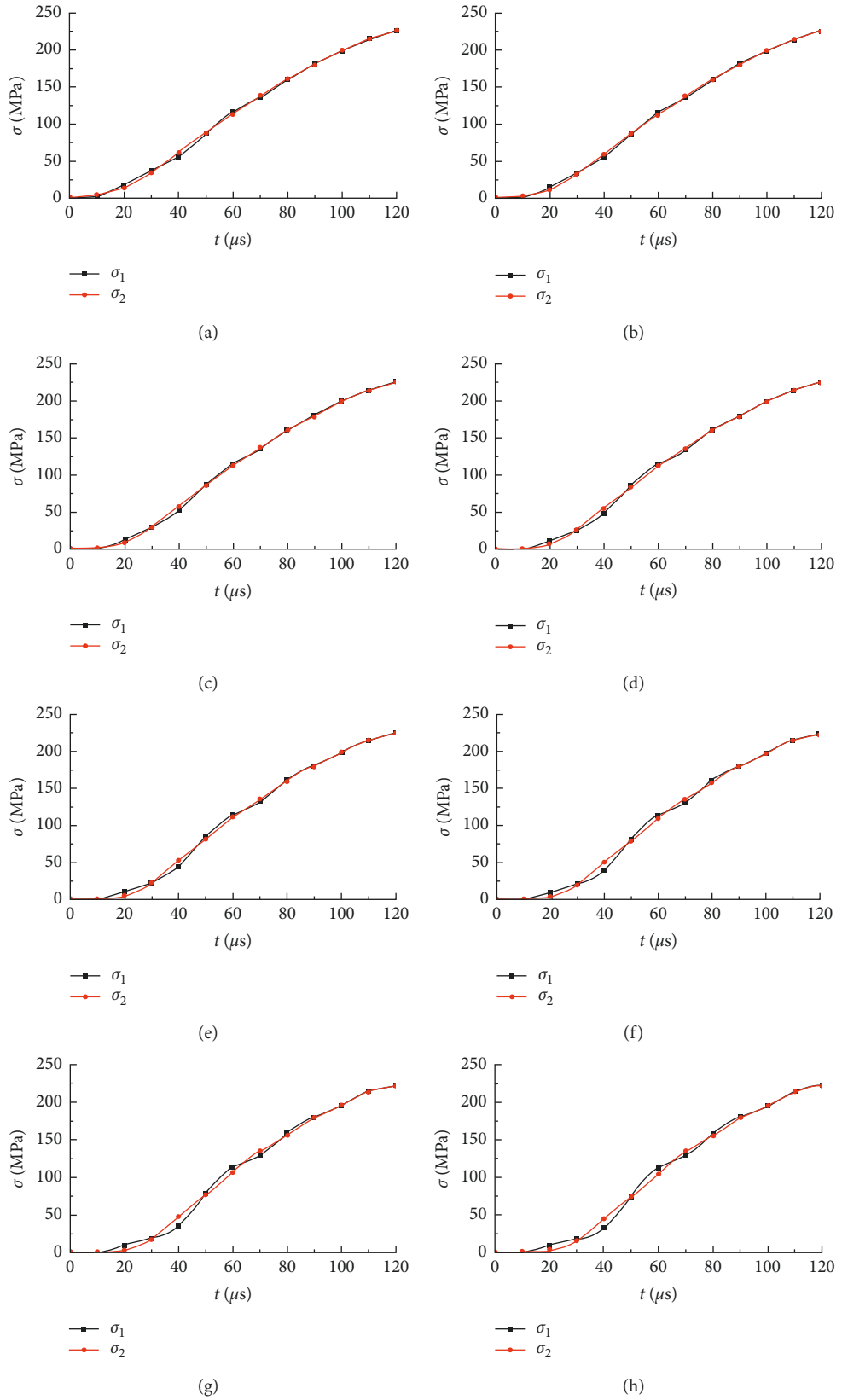

Figure 6: Continued.

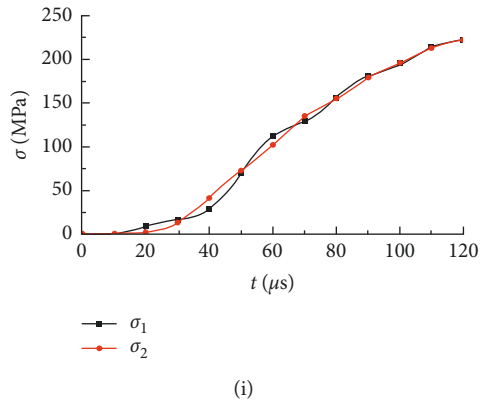

(i)

Figure 6: Stress history on two ends of nonparallel end-surface rock specimens when Young's modulus is 28 GPa: (a) $\gamma = 0\%$, (b) $\gamma = 0.05\%$, (c) $\gamma = 0.10\%$, (d) $\gamma = 0.15\%$, (e) $\gamma = 0.20\%$, (f) $\gamma = 0.25\%$, (g) $\gamma = 0.30\%$, (h) $\gamma = 0.35\%$, and (i) $\gamma = 0.40\%$.

While for nonparallel end-surface rock specimens, the contact area is a part of circular section for a tiny gap between the rock specimen and transmission bar. When incident stress propagates to this place, most of the incident stress is reflected for the less contact area of the nonparallel end-surface, and the contact area at the nonparallel contact surface becomes larger for compressive deformation of the rock specimen under transmitted stress. Reflected stress and transmitted stress propagate along a certain angle to the axis for the nonparallel end-surface. After repeated reflection and transmission between two ends of rock specimen, a slight fluctuation presents for propagation direction deviation. Due to the parallel contact surface between the incident bar and rock specimen, distorted reflected stress caused by the nonparallel contact surface can be well transmitted into the incident bar. Therefore, reflected stress presents a relatively obvious fluctuation effect. Moreover, the fluctuation effect is enhanced with end-surface nonparallelism for both reflected stresses and transmitted stresses.

During stress wave propagation, the compressive deformation can compensate for the tiny gap between the rock specimen and transmission bar. On one hand, the compressive deformation can weaken the distorted reflected stress from the nonparallel contact surface, which means a weak fluctuation effect in reflected stresses. On the other hand, the compressive deformation can enhance the fluctuation effect in transmitted stress for the unstable contact area between the rock specimen and transmission bar during repeated reflection and transmission in rock specimen. It is well known that compressive deformation is related to its Young's modulus. Hence, the fluctuation effect in reflected stresses is enhanced with Young's modulus, while the fluctuation effect in transmitted stresses is weakened with Young's modulus.

3.3. Stress History on Two Ends of Rock Specimens. When Young's modulus is 28 GPa, stress history on two ends of nonparallel end-surface rock specimens are presented in Figure 6. Stress history on the end contacted with the incident bar is marked as $\sigma_1(t)$, and stress history on the end contacted with the transmission bar is marked as $\sigma_2(t)$. $\sigma_1(t)$ and $\sigma_2(t)$ can be derived from incident, reflected, and transmitted stresses by the following equations:

$$\begin{aligned} \sigma_1(t) &= -\sigma_I(t) - \sigma_R(t), \\ \sigma_2(t) &= -\sigma_T(t). \end{aligned} \tag{4}$$

As shown in Figure 6(a), the noncoincidence between the stress history on two ends of parallel end-surface rock specimen is mainly in the initial loading stage, and the difference is very small. As shown in Figures 6(b)–6(i), the noncoincidence between the stress history on two ends of nonparallel end-surface rock specimens is extended with the increase of end-surface nonparallelism in loading process, and the difference is also enlarged. Comparing Figure 6(a) with Figures 6(b) and 6(c), it can be found that the difference of stress history on two ends of nonparallel end-surface specimen is smaller than that for parallel end-surface rock specimen when end-surface nonparallelism not exceeds 0.10%.

To analyze the difference between stress history on two ends quantitatively, stress deviation history $\Delta\sigma(t)$ between stress history on two ends is involved and can be calculated by $\sigma_1(t)$ substracting $\sigma_2(t)$. The stress deviation history $\Delta\sigma(t)$ for various end-surface nonparallelisms and various Young's moduli are shown in Figure 7. And the maximum stress deviation $\Delta\sigma_{max}$ for each condition is scattered in Figure 8.

As shown in Figure 7, stress deviation history $\Delta\sigma(t)$ presents a wave trend with the loading time, and stress deviation achieves its maximum value at about 40 μs. Under the same Young's modulus, the amplitude of stress deviation history $\Delta\sigma(t)$ increases with the increase of end-surface nonparallelism. Under the same end-surface nonparallelism, the amplitude of stress deviation history decreases with the increase of Young's modulus.

As shown in Figure 8, under the same Young's modulus, the maximum stress deviation $\Delta\sigma_{max}$ first decreases then increases with the increase of end-surface nonparallelism and reaches its lowest value at end-surface nonparallelism of 0.05%. This may be explained by the fact that the dispersion effect in SHPB test is further weakened by the fluctuation effect and shifting in reflected

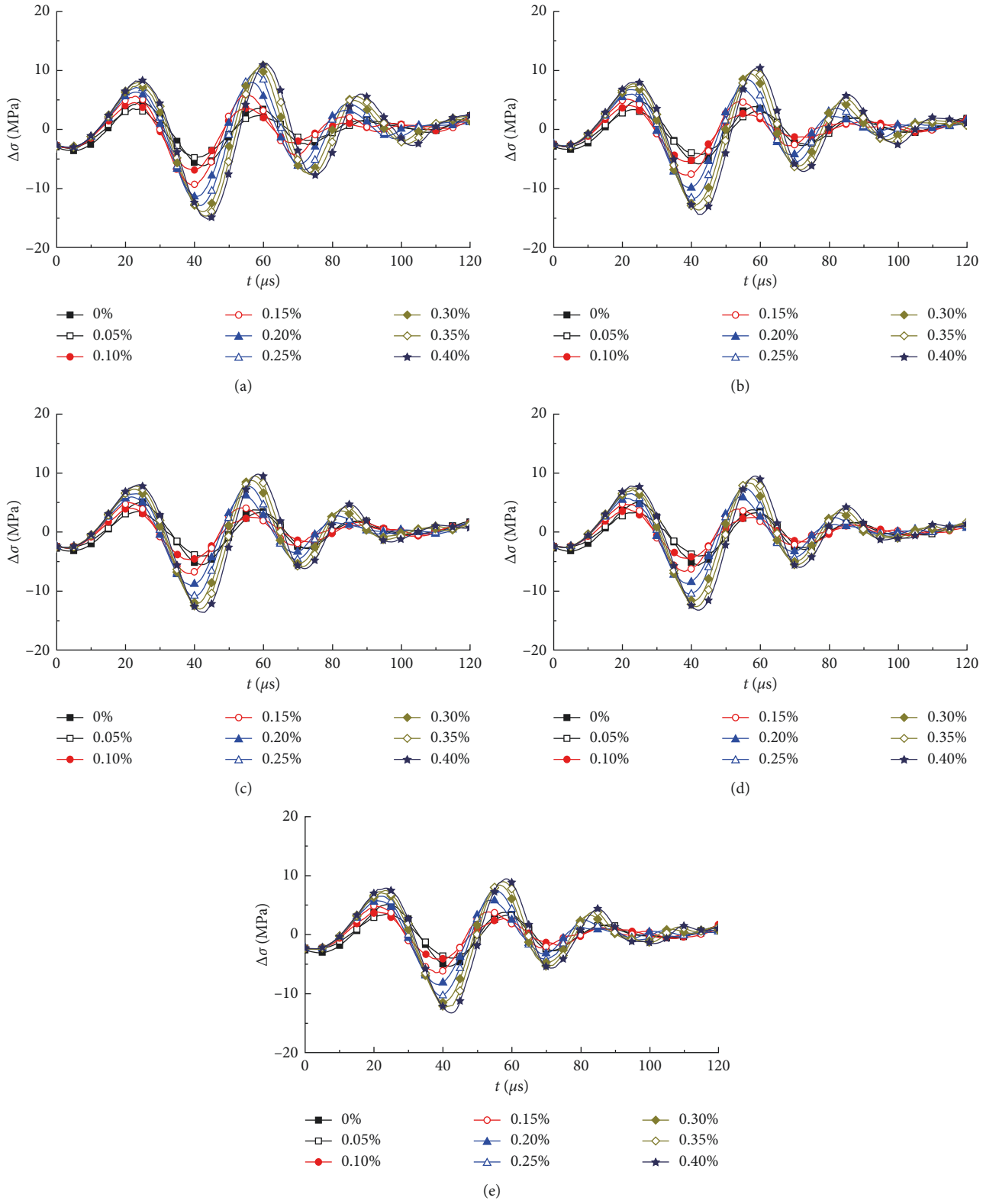

Figure 7: Stress deviation history $\Delta\sigma(t)$ for various end-surface nonparallelisms and Young's moduli: (a) $E = 14$ GPa, (b) $E = 21$ GPa, (c) $E = 28$ GPa, (d) $E = 35$ GPa, and (e) $E = 42$ GPa.

stresses and transmitted stresses. Meanwhile, the maximum stress deviation $\Delta\sigma_{max}$ shows a little difference when end-surface nonparallelism is within 0.10%. Under the same end-surface nonparallelism, the maximum stress deviation $\Delta\sigma_{max}$ decreases with the increase of Young's modulus.

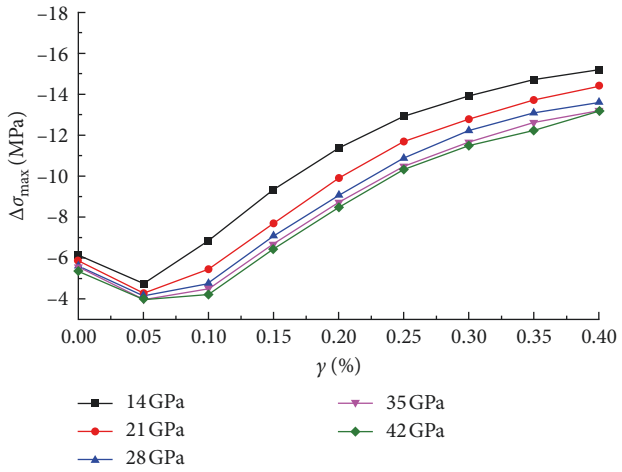

Figure 8: Relation between maximum stress deviation $\Delta\sigma_{max}$ and end-surface nonparallelism γ.

4. Effect of Nonparallel End-Surface on Stress Uniformity during Loading Process

4.1. Stress Nonuniformity Coefficient. Stress nonuniformity coefficient $\alpha(t)$ is adopted to describe the stress uniformity during loading process in SHPB tests, and it can be derived by dividing absolute value of stress deviation to average value of stress history on two ends [16–18]. Stress nonuniformity coefficient $\alpha(t)$ can be calculated by the following equation:

$$\alpha(t) = \left|\frac{\sigma_1(t) - \sigma_2(t)}{(\sigma_1(t) + \sigma_2(t))/2}\right| = \left|\frac{-\sigma_I(t) - \sigma_R(t) + \sigma_T(t)}{(-\sigma_I(t) - \sigma_R(t) - \sigma_T(t))/2}\right| = \left|\frac{\sigma_I(t) + \sigma_R(t) - \sigma_T(t)}{(\sigma_I(t) + \sigma_R(t) + \sigma_T(t))/2}\right|. \quad (5)$$

Stress nonuniformity coefficient $\alpha(t)$ reflects the state of stress uniformity of rock specimens at various loading times. The closer the stress uniformity nonuniformity coefficient $\alpha(t)$ to 0 is, the more uniform the internal stress in the rock specimen is. Stress nonuniformity coefficient $\alpha(t)$ for various end-surface nonparallelisms and various Young's moduli are shown in Figure 9.

As shown in Figure 9, under the same Young's modulus, stress nonuniformity coefficient $\alpha(t)$ for various end-surface nonparallelism attenuates in a serrated fluctuation with the increase of loading time. And stress nonuniformity coefficient $\alpha(t)$ increases with the increase of end-surface nonparallelism. The influence of end-surface nonparallelism on stress nonuniformity coefficient $\alpha(t)$ is weakened with loading time going on and mainly concentrates on the first 70 μs of loading process.

4.2. Stress Equilibrium Time. When stress nonuniformity coefficient $\alpha(t)$ is equal to or less than 0.05, it is considered that the stress equilibrium state is achieved in loading process and the stress distribution in rock specimen meets the assumption of stress uniformity. Stress equilibrium time, marked as t_u, is defined as the time spent from the start of loading to the stress nonuniformity coefficient $\alpha(t)$ equal to or less than 0.05 [17]. Stress equilibrium time t_u for each condition is scattered in Figure 10.

As shown in Figure 10, under the same Young's modulus, the stress equilibrium time t_u first decreases then increases in a step type with the increase of end-surface nonparallelism. Therefore, nonparallel end-surface leads to two reverse results for stress uniformity during SHPB loading process, to extend stress equilibrium time and to shorten stress equilibrium time. When end-surface nonparallelism is 0.10%, stress equilibrium time achieves its lowest value whatever the Young's modulus is. And the lowest stress equilibrium time for Young's modulus of 14 GPa, 21 GPa, 28 GPa, 35 GPa, and 42 GPa are 46.2 μs, 44.5 μs, 43.7 μs, 42.6 μs, and 42.2 μs, respectively.

4.3. Influence of End-Surface Nonparallelism on Stress Uniformity

4.3.1. $\gamma \le 0.10\%$. As shown in Figure 10, when end-surface nonparallelism is equal to or less than 0.10%, the stress equilibrium time slightly reduces with the increase of end-surface nonparallelism. Therefore, the influence of end-surface nonparallelism on stress equilibrium time is very small. Meanwhile, Young's modulus also presents little influence on stress equilibrium time. The stress equilibrium time also slightly reduces with the increase of Young's modulus.

Due to the fluctuation effect and shifting in reflected stresses and transmitted stresses, the dispersion effect in SHPB test is further weakened. Meanwhile, both stress deviation and average stress of two ends are changed. It is considered that the tiny gap between the rock specimen and transmission bar can improve the stress distribution in rock specimens during loading process in SHPB tests. When end-surface nonparallelism is equal to or less than 0.10%, nonparallel end-surface can shorten the stress equilibrium time, avoid premature failure of rock-like materials, and improve stress uniformity of rock specimen. Compared with the parallel end-surface rock specimen, the stress equilibrium time for the rock specimen with end-surface nonparallelism of 0.10% is reduced by 4.3%, 5.7%, 5.8%, 6.8%, and 7.0% corresponding to Young's modulus of 14 GPa, 21 GPa, 28 GPa, 35 GPa, and 42 GPa. The effect of nonparallel end-surface is very small, which can be negligible. Hence, end-surface nonparallelism of rock specimen is suggested to be controlled within 0.10% when conducting SHPB tests.

4.3.2. $0.10\% \le \gamma \le 0.40\%$. As shown in Figure 10, when end-surface nonparallelism ranges from 0.10% to 0.40%, the stress equilibrium time increases in a step type. And step change range varies for various Young's moduli. For Young's modulus of 14 GPa, one step change occurs when end-surface nonparallelism ranges from 0.10% to 0.20%. For Young's modulus of 21 GPa, two step changes occur when

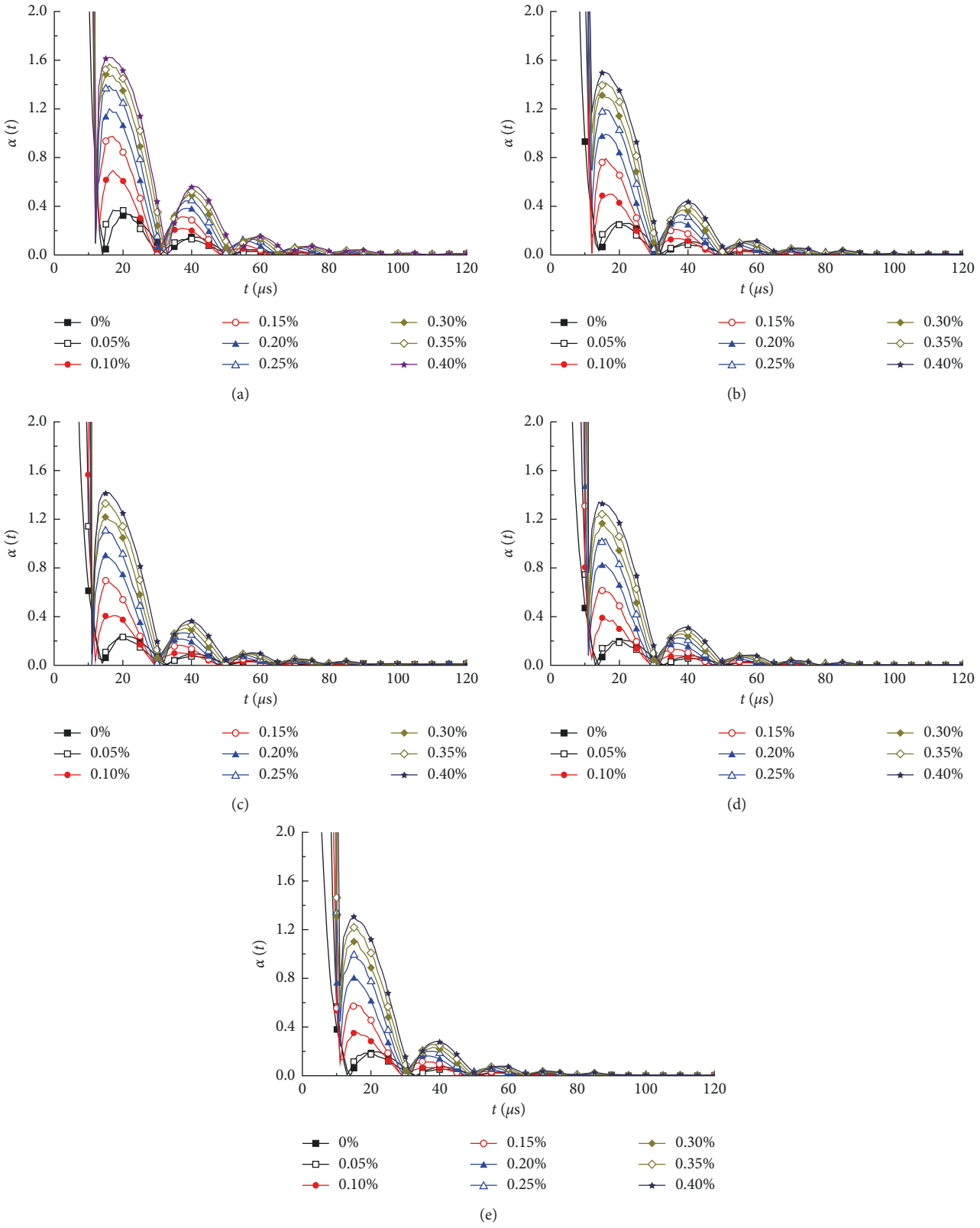

FIGURE 9: Stress nonuniformity coefficient $\alpha(t)$ for various end-surface nonparallelisms and Young's moduli: (a) $E = 14$ GPa, (b) $E = 21$ GPa, (c) $E = 28$ GPa, (d) $E = 35$ GPa, and (e) $E = 42$ GPa.

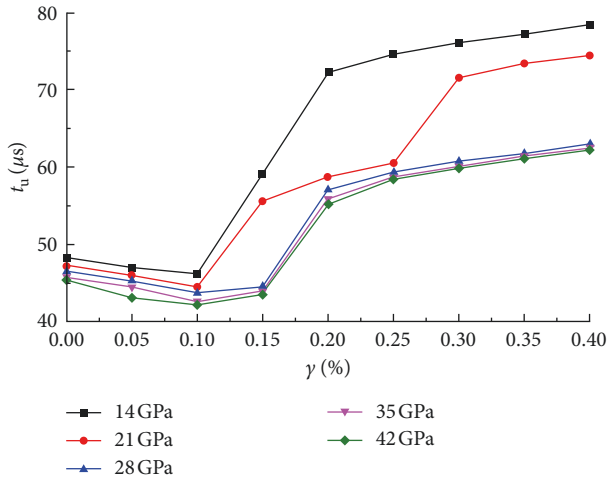

Figure 10: Relation between stress equilibrium time t_u and end-surface nonparallelism γ.

end-surface nonparallelism ranges from 0.10% to 0.15% and from 0.25% to 0.30%. When Young's modulus is equal to or greater than 28 GPa, one step change occurs when end-surface nonparallelism ranges from 0.15% to 0.20%. Moreover, growth rates of stress equilibrium time in step change range are similar for different Young's moduli. When end-surface nonparallelism increases 0.05%, average growth rates of stress equilibrium time in step change range are 28.2%, 21.6%, 28.3%, 27.3%, and 26.9% corresponding to Young's modulus of 14 GPa, 21 GPa, 28 GPa, 35 GPa, and 42 GPa.

Under the same end-surface nonparallelism, stress equilibrium time decreases with the increase of Young's modulus. And the descent of stress equilibrium time is mainly occurred when Young's modulus ranges from 14 GPa to 28 GPa. When Young's modulus is equal to or greater than 28 GPa, the stress equilibrium times for various Young's moduli are roughly the same. When end-surface nonparallelism is 0.30%, the stress equilibrium time are 76.1 μs, 71.6 μs, 60.7 μs, 60.1 μs, and 59.9 μs corresponding to Young's modulus of 14 GPa, 21 GPa, 28 GPa, 35 GPa, and 42 GPa. It can be found that when Young's modulus is ranging from 28 GPa to 42 GPa, the influence of Young's modulus on stress equilibrium time is very small and can be negligible.

5. Conclusions

(1) Fluctuation effect exists in both reflected stresses and transmitted stresses, and it is enhanced with the increase of end-surface nonparallelism. With the increase of Young's modulus, the fluctuation effect in reflected stresses is enhanced, while the fluctuation effect in transmitted stresses is weakened. Under the same Young's modulus, the amplitude of reflected stresses gradually rises, while the amplitude of transmitted stresses gradually decreases with the increase of end-surface nonparallelism.

(2) Stress deviation history presents a wave trend with the loading time, and stress deviation achieves its maximum value at about 40 μs. Under the same Young's modulus, the amplitude of stress deviation history increases with the increase of end-surface nonparallelism. Under the same end-surface nonparallelism, the amplitude of stress deviation history decreases with the increase of Young's modulus.

(3) Under the same Young's modulus, stress nonuniformity coefficient for various end-surface nonparallelism attenuates in a serrated fluctuation with the increase of loading time. And stress nonuniformity coefficient increases with the increase of end-surface nonparallelism. The influence of end-surface nonparallelism on stress nonuniformity coefficient is weakened with loading time going on, and it mainly concentrates on the first 70 μs of loading process.

(4) Under the same Young's modulus, the stress equilibrium time first decreases slightly then increases in a step type with the increase of end-surface nonparallelism. When end-surface nonparallelism is 0.10%, stress equilibrium time achieves its lowest value whatever the Young's modulus is. When Young's modulus exceeds 28 GPa, the influence of Young's modulus on stress equilibrium time can be negligible.

(5) Nonparallel end-surface leads to two reverse results for stress uniformity during SHPB loading process. One is extending stress equilibrium time, and the other is shortening stress equilibrium time. Influence on shortening stress equilibrium time is weak and can be negligible, while influence on extending stress equilibrium time is great. Hence, end-surface nonparallelism of rock specimen is suggested to be controlled within 0.10% when conducting SHPB tests.

Data Availability

The datasets generated and analyzed during the current study are available from the corresponding author on reasonable request.

Conflicts of Interest

The authors declare that there are no conflicts of interest regarding the publication of this paper.

Acknowledgments

This research was funded by National Natural Science Foundation of China (no. 51774011), Anhui Provincial Natural Science Foundation (no. 1808085QE148), Natural Science Research Project of Colleges and Universities in Anhui Province (no. KJ2017A097), Young Teacher Scientific Research Project of Anhui University of Science and Technology (no. QN201607), Science and Technology Project of Department of Housing and Urban-Rural Development of Anhui Province (no. 2017YF-08), and Opening Project Fund of State Key Laboratory of Mining Disaster

Prevention and Control cofounded by Shandong Province and the Ministry of Science and Technology (no. MDPC201603).

References

[1] Q. B. Zhang and J. Zhao, "A review of dynamic experimental techniques and mechanical behaviour of rock materials," *Rock Mechanics and Rock Engineering*, vol. 47, no. 4, pp. 1411–1478, 2014.

[2] Z. L. Zhou, Y. Zhao, Y. H. Jiang et al., "Dynamic behavior of rock during its post failure stage in SHPB tests," *Transactions of Nonferrous Metals Society of China*, vol. 27, no. 1, pp. 184–196, 2017.

[3] T. C. Yet, R. Hamid, and M. Kasmuri, "Dynamic stress-strain behaviour of steel fiber reinforced high-performance concrete with fly ash," *Advances in Civil Engineering*, vol. 2012, Article ID 907431, 6 pages, 2012.

[4] D. D. Ma, Q. Y. Ma, and P. Yuan, "SHPB tests and dynamic constitutive model of artificial frozen sandy clay under confining pressure and temperature state," *Cold Regions Science and Technology*, vol. 136, pp. 37–43, 2017.

[5] P. Yuan and Y. Xu, "Influence of curing time on impact energy absorption characteristics of artificially cemented sand," *Journal of Vibroengineering*, vol. 19, no. 6, pp. 4033–4041, 2017.

[6] J. L. Tao, *SHPB Experimental Technique*, Science Press, Beijing, China, 2014.

[7] W. Z. Zhong, A. Rusine, T. Jankowiak et al., "Influence of interfacial friction and specimen configuration in split Hopkinson pressure bar system," *Tribology International*, vol. 90, pp. 1–14, 2015.

[8] M. A. Kariem, J. H. Beynon, and D. Ruan, "Misalignment effect in the split Hopkinson pressure bar technique," *International Journal of Impact Engineering*, vol. 47, pp. 60–70, 2012.

[9] X. Wu, Q. Yin, Y. Wei et al., "Effects of imperfect experimental conditions on stress waves in SHPB experiments," *Acta Mechanica Sinica*, vol. 31, no. 6, pp. 827–836, 2015.

[10] Z. L. Zhou, L. Hong, Q. Y. Li et al., "Calibration of split Hopkinson pressure bar system with special shape striker," *Journal of Central South University of Technology*, vol. 18, no. 4, pp. 1139–1143, 2011.

[11] Y. X. Zhou, K. Xia, X. B. Li et al., "Suggested methods for determining the dynamic strength parameters and mode-I fracture toughness of rock materials," *International Journal of Rock Mechanics and Mining Sciences*, vol. 49, pp. 105–112, 2012.

[12] F. Dai, S. Huang, K. Xia et al., "Some fundamental issues in dynamic compression and tension tests of rocks using split Hopkinson pressure bar," *Rock Mechanics and Rock Engineering*, vol. 43, no. 6, pp. 657–666, 2010.

[13] P. Yuan and Q. Y. Ma, "Correction of non-parallel end-faces of rock specimens in SHPB tests," *Explosion and Shock Waves*, vol. 37, no. 5, pp. 929–936, 2017.

[14] G. M. Zhao, W. W. Ma, and X. R. Meng, "Damage modes and energy characteristics of rock-like materials under dynamic load," *Rock and Soil Mechanics*, vol. 36, no. 12, pp. 3598–3605, 2015.

[15] J. C. Li, N. N. Li, H. B. Li et al., "An SHPB test study on wave propagation across rock masses with different contact area ratios of joint," *International Journal of Impact Engineering*, vol. 105, pp. 109–116, 2017.

[16] J. Zhu, S. S. Hu, and L. L. Wang, "An analysis of stress uniformity for concrete-like specimens during SHPB tests," *International Journal of Impact Engineering*, vol. 36, no. 1, pp. 61–72, 2009.

[17] L. M. Yang and V. P. Shim, "An analysis of stress uniformity in split Hopkinson bar test specimens," *International Journal of Impact Engineering*, vol. 31, no. 2, pp. 129–150, 2005.

[18] Q. Ping, Q. Y. Ma, and P. Yuan, "Stress equilibrium in rock specimen during the loading process of SHPB experiment," *Explosion and Shock Waves*, vol. 33, no. 6, pp. 655–661, 2013.